ONE-DIMENSIONAL ANALYSIS OF FULL LOAD DRAFT TUBE SURGE CONSIDERING THE FINITE SOUND VELOCITY IN THE PENSTOCK

AUTHORS

Changkun CHEN
Engineering Science, Osaka University
Osaka, Japan
chenchangkun@mbox.me.es.osaka-u.ac.jp

Christophe NICOLET
Laboratory for Hydraulic Machines, EPFL, Lausanne, Switzerland
christophe.nicolet@epfl.ch

Koichi YONEZAWA
Engineering Science, Osaka University
Osaka, Japan
yonezawa@me.es.osaka-u.ac.jp

Mohamed FARHAT
Laboratory for Hydraulic Machines, EPFL, Lausanne, Switzerland
Mohamed.Farhat@epfl.ch

Francois AVELLAN
Laboratory for Hydraulic Machines, EPFL, Lausanne, Switzerland
francois.avellan@epfl.ch

Yoshinobu TSUJIMOTO
Engineering Science, Osaka University
Osaka, Japan
tujimoto@me.es.osaka-u.ac.jp

ABSTRACT

A previous report by the present authors [1] clarified the diffuser effect of the draft tube and the effects of swirl in the runner downstream on the hydraulic instabilities in power generation plants. The present study was intended to study the effect of finite sound velocity in the penstock, based on a similar one-dimensional analytical model as Ref. [1]. It was found that the introduction of finite sound velocity in the penstock results in the occurrence of higher order frequency modes. The diffuser and swirl effects on each frequency mode are examined in the present study.

KEY WORD: Draft tube surge, finite sound velocity, higher order frequencies

INTRODUCTION

Draft tube surge at off-design conditions is one of the most important phenomena in Francis turbines. At part load operation, it has been clarified that it is caused by the resonance of hydraulic system with the precession motion of vortex rope in the draft tube [2]-[5]. At full load operation, the surge is self-excited but the cause was not clear. References [6] and [7] show that full load surge can be successfully simulated by using appropriate values of mass flow gain factor and cavitation compliance to represent the cavitation effect in the draft tube. However, the flow mechanism determining the value of mass flow gain factor was not clear. In the previous study [1], a one dimensional analytical model was built to study the mechanism of full load draft tube surge, assuming an incompressible flow in the penstock. It was found that the diffuser effect of the draft tube has a destabilizing effect over all flow rates, while the swirl effects stabilize/destabilize the system at larger/smaller flow rates than the swirl free flow rate. The present study was carried out in order to clarify the effect of finite sound velocity in the penstock.

NOMENCLATURE

Standard Value			
a = 500 [m/s]	Wave speed in the penstock	S = 0.125 [m^2]	Runner exit area
A_c = 0.125 [m^2]	Draft tube inlet area	u	Flow velocity
A_i = 0.22 [m^2]	Inlet pipe area	U_2 = 15.7 [m/s]	Runner exit circumferential velocity
A_e = 0.67 [m^2]	Draft tube exit area	V_c	Volume of cavity
C = 97.2×10^{-7} [m^{4}s^2/kg]	Cavitation compliance		
$D = (A_e/A_c)^2$-1=27.7 [-]	Diffusion factor of draft tube	α = 10 [-]	Pressure coefficient of swirl
H = 14.8 [m]	Head	β_2 = 17.5 [degree]	Runner exit blade angle
L_e = 4.36 [m]	Effective length of draft tube	ρ = 1000 [kg/m^3]	Fluid density
L_i = 50 [m]	Inlet pipe length	$\omega = \omega_R + j\omega_I$	Complex frequency
p	Pressure	ω_e = 12.56 [rad/s]	Draft tube resonance frequency
Q = 0.51 [m^3/s]	Flow rate	ζ_2 = 0.207 [-]	Loss coefficient of draft tube
Q_{sf} = 0.618 [m^3/s]	Swirl free flow rate	ζ_T = 54.2 [-]	Runner resistance

ANALYTICAL MODEL AND EQUATIONS

As shown in Fig. 1, we consider the same system as [1], which is composed of an inlet pipe of length L_i and area A_i, a turbine runner, and a draft tube with the inlet and exit areas A_c and A_e, respectively. A cavity of volume V_c is assumed downstream of the turbine and upstream of the draft tube. Then, the continuity equation between upstream and downstream flow rates Q_1 and Q_2 is:

$$Q_2 - Q_1 = dV_c / dt \qquad (1)$$

By applying Bernoulli's equation to the draft tube, we obtain,

$$p_a = p_{exit} + \rho \frac{L_e}{A_e} \frac{dQ_2}{dt} + \rho \frac{\zeta_2 - D}{2A_e^2} Q_2^2 \qquad (2)$$

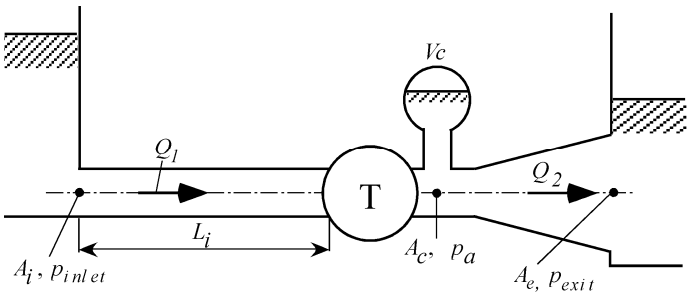

Fig. 1 Hydraulic system for the analysis

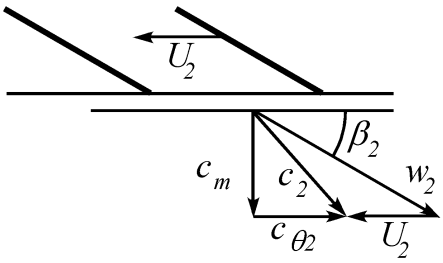

Fig. 2 Velocity triangle at the runner exit

where $L_e = \int (A_e / A(s))ds$ is the effective length of the draft tube, $D=(A_e/A_c)^2-1$ the diffuser factor, ζ_2 the loss coefficient of the draft tube. For simplicity, ζ_2 is assumed to be constant although it may depend on the swirl of the discharge flow [8]. Equation (2) ignores the flow compressibility in the draft tube.

At off-design operating point, the discharge flow from the runner swirls and a vortex is formed. If the pressure p_c at the vortex center is lower than the vapor pressure, a cavity will appear. The volume of cavity can be considered to be a function of the core pressure p_c,

$$V_c = V_c(p_c) \qquad (3)$$

Due to the centrifugal force on the swirling flow, the core pressure p_c is lower than the ambient pressure p_a and can be expressed

$$p_c = p_a - \rho\alpha c_{\theta 2}^2 \qquad (4)$$

Here, $c_{\theta 2}$ is a representative swirl velocity and α is a pressure coefficient for the swirl effects. If we assume a Rankine's combined vortex with the core radius r and the outer radius R, α is determined to be $\alpha=(R/r)^2-1/2$, with $c_{\theta 2}$ evaluated at the outer radius R, although the real flow from the runner is much more complicated [8].

From the velocity triangle at the runner discharge as shown in Fig. 2, we obtain

$$c_{\theta 2} = c_{m2}\cot\beta_2 - U_2 = \frac{Q_1}{S}\cot\beta_2 - U_2 \qquad (5)$$

where β_2 is the runner exit vane angle, S the runner exit area and U_2 the runner exit peripheral speed.

By putting Eqs. (2) and (5) in Eq. (4), we obtain

$$p_c = p_{exit} + \rho\frac{L_e}{A_e}\frac{dQ_2}{dt} + \rho\frac{\zeta_2 - D}{2A_e^2}Q_2^2 - \rho\alpha\left(\frac{\cot\beta_2}{S}Q_1 - U_2\right)^2 \qquad (6)$$

The cavitation compliance C is defined by

$$C = -dV_c / dp_c \qquad (7)$$

Then, the continuity equation (1) can be expressed as

$$Q_2 - Q_1 = dV_c/dt = (dV_c/dp_c)(dp_c/dt) = -C(dp_c/dt)$$

$$= -\rho C\frac{L_e}{A_e}\frac{d^2Q_2}{dt^2} + \rho C\frac{D-\zeta_2}{A_e^2}Q_2\frac{dQ_2}{dt} + 2\rho C\alpha\frac{\cot\beta_2}{S}\left(\frac{\cot\beta_2}{S}Q_1 - U_2\right)\frac{dQ_1}{dt} \qquad (8)$$

The second term with dQ_2/dt represents the diffuser effect corresponding to the mass flow gain factor. If the discharge flow Q_2 is increased, the ambient pressure p_a is decreased if the diffuser effect D is larger than the loss ζ_2, resulting in an increase in cavity volume, which would promote further increase of Q_2. The third term with dQ_1/dt represents the effect of swirl. This term may also be called "mass flow gain factor" but this term is associated with the upstream flow Q_1. At flow rates lower than design ($Q_1<Q_{sf}=U_2S\tan\beta_2$), the tangential velocity $c_{\theta 2}$ and the cavity volume decrease as the upstream flow rates Q_1 is increased. This would promote further increas in Q_1.

Considering the compressibility of the fluid and the elasticity of pipe wall, the momentum and continuity equations applied to the flow in upstream penstock are

$$\frac{\partial u}{\partial t} + \frac{1}{\rho}\frac{\partial p}{\partial x} = 0 \qquad (9)$$

$$\frac{\partial p}{\partial t} + \rho a^2 \frac{\partial u}{\partial x} = 0 \quad (10)$$

where a is the wave speed and can be evaluated from the speed of sound and the geometry of penstock section. The convective term has been ignored as being small with respect to other terms.

By taking the partial derivative of Eq. (10) with respect to t and Eq. (9) with respect to x, one may eliminate u, which yields

$$\frac{\partial^2 p}{\partial t^2} - a^2 \frac{\partial^2 p}{\partial x^2} = 0 \quad (11)$$

In a similar manner, p may be eliminated, giving

$$\frac{\partial^2 u}{\partial t^2} - a^2 \frac{\partial^2 u}{\partial x^2} = 0 \quad (12)$$

The general solutions of Eqs. (9)- (12) can be expressed as

$$\begin{cases} p = R\left(t - \frac{x}{a}\right) + L\left(t + \frac{x}{a}\right) \\ \rho a u = R\left(t - \frac{x}{a}\right) - L\left(t + \frac{x}{a}\right) \end{cases}$$

The function $R\left(t - \frac{x}{a}\right)$ expresses a wave propagating towards positive x and $L\left(t + \frac{x}{a}\right)$ is another wave towards negative x. For the stability analysis, we separate each quantity into steady and unsteady components: $Q = \bar{Q} + \tilde{Q}(t)$, $p = \bar{p} + \tilde{p}(t)$ and $u = \bar{u} + \tilde{u}(t)$. The absolute value of steady part is assumed to be much larger than unsteady part. Only taking the unsteady part into account, we can assume the general solutions as:

$$\tilde{p} = p_R \cdot e^{j\omega\left(t - \frac{x}{a}\right)} + p_L \cdot e^{j\omega\left(t + \frac{x}{a}\right)} \quad (13)$$

$$\rho a \tilde{u} = p_R \cdot e^{j\omega\left(t - \frac{x}{a}\right)} - p_L \cdot e^{j\omega\left(t + \frac{x}{a}\right)} \quad (14)$$

Solutions (13) and (14) satisfy Eqs. (11) and (12) generally even with a complex value of ω. Assuming no pressure fluctuation ($\tilde{p} = 0$) at the entrance of the inlet pipe (x = 0), we can obtain p_R + p_L =0 from Eq. (13). By putting this result back into Eqs. (13) and (14), we obtain the pressure and velocity fluctuations along the inlet pipe

$$\tilde{p} = p_R e^{j\omega t}\left(e^{-j\omega\frac{x}{a}} - e^{j\omega\frac{x}{a}}\right) = -2j \cdot p_R e^{j\omega t} \sin\left(\omega \frac{x}{a}\right) \quad (15)$$

$$\rho a \tilde{u} = p_R e^{j\omega t}\left(e^{-j\omega\frac{x}{a}} + e^{j\omega\frac{x}{a}}\right) = 2 \cdot p_R e^{j\omega t} \cos\left(\omega \frac{x}{a}\right) \quad (16)$$

By combining Eqs. (15) and (16), the pressure fluctuation can be correlated with the velocity fluctuation. The pressure fluctuation $\tilde{p}_{inlet}$ at the inlet of the runner $x = L_i$ can be correlated with the velocity fluctuation $\tilde{u}_{inlet}$:

$$\tilde{p}_{inlet} = -j \cdot \rho a \tan\left(\omega \frac{L_i}{a}\right) \cdot \tilde{u}_{inlet} \quad (17)$$

We assume that the pressure difference between the inlet and exit of runner can be present by

$$p_{inlet} - p_a = \frac{\rho}{2} \zeta_T u_{inlet}^2 = \frac{\rho}{2} \zeta_T \left(\bar{u}_{inlet}^2 + 2\bar{u}_{inlet}\tilde{u}_{inlet} + \tilde{u}_{inlet}^2\right)$$

where p_a is the pressure at the turbine discharge and ζ_T is a coefficient which represents the effect of runner. The unsteady part is

$$\tilde{p}_{inlet} - \tilde{p}_a = \rho \zeta_T \bar{u}_{inlet} \tilde{u}_{inlet} = \frac{\rho \zeta_T}{A_i^2} \bar{Q}_1 \tilde{Q}_1 \quad (18)$$

The unsteady part of Bernoulli's equation (2) applied to the draft tube is

$$\tilde{p}_a = \tilde{p}_{exit} + \frac{\rho L_e}{A_e} j\omega \tilde{Q}_2 + \frac{\rho(\zeta_2 - D)}{A_e^2} \bar{Q}_2 \tilde{Q}_2 \quad (19)$$

By applying Eqs. (18) and (19) into (17), we obtain

$$-j \cdot \rho a \tan\left(\omega \frac{L_i}{a}\right) \cdot \frac{\tilde{Q}_1}{A_i} - \left(\frac{\rho L_e}{A_e} j\omega \tilde{Q}_2 + \frac{\rho(\zeta_2 - D)}{A_e^2} \bar{Q}_2 \tilde{Q}_2 \right) = \frac{\rho \zeta_T}{A_i^2} \bar{Q}_1 \tilde{Q}_1$$

Which can be reduced to

$$\tilde{Q}_1 = -\frac{\frac{\rho L_e}{A_e} j\omega + \frac{\rho(\zeta_2 - D)}{A_e^2} \bar{Q}_2}{\frac{\rho \zeta_T}{A_i^2} \bar{Q}_1 + j \cdot \frac{\rho a}{A_i} \tan\left(\omega \frac{L_i}{a}\right)} \tilde{Q}_2 \quad (20)$$

The unsteady part of continuity equation (8) between upstream and downstream flow rates Q_1 and Q_2 is

$$\tilde{Q}_2 - \tilde{Q}_1 = -\frac{\rho L_e C}{A_e} \frac{d^2 \tilde{Q}_2}{dt^2} + \frac{\rho C}{A_e^2}(D - \zeta_2) \bar{Q}_2 \frac{d\tilde{Q}_2}{dt} + \frac{2\rho C \alpha \cot \beta_2}{S} \left(\frac{\cot \beta_2}{S} \bar{Q}_1 - u_2 \right) \cdot \frac{d\tilde{Q}_1}{dt} \quad (21)$$

By applying Eq. (20) into (21) and using $\tilde{Q}_1 = A_i \tilde{u}_l$, the system characteristic equation assuming the finiteness of sound velocity in the penstock is obtained:

$$\begin{aligned}
&\left(\frac{\rho a}{A_i} \frac{\rho L_e}{A_e} jC \right) \omega^2 \tan\left(\omega \frac{L_i}{a}\right) \\
&+ \left[\frac{\rho \zeta_T}{A_i^2} \bar{Q}_1 \cdot \frac{\rho L_e C}{A_e} + \frac{2\rho C \alpha \cot \beta_2}{S} \left(\frac{\cot \beta_2}{S} \bar{Q}_1 - u_2 \right) \cdot \frac{\rho L_e}{A_e} \right] \omega^2 - \left[\frac{\rho a}{A_i} \frac{\rho C}{A_e^2} (D - \zeta_2) \bar{Q}_2 \right] \omega \tan\left(\omega \frac{L_i}{a}\right) \\
&+ \left[-\frac{\rho L_e}{A_e} j + \frac{\rho \zeta_T}{A_i^2} \bar{Q}_1 \cdot \frac{\rho C}{A_e^2} (D - \zeta_2) \bar{Q}_2 j - \frac{2\rho C \alpha \cot \beta_2}{S} \left(\frac{\cot \beta_2}{S} \bar{Q}_1 - u_2 \right) \cdot \frac{\rho(\zeta_2 - D)}{A_e^2} \bar{Q}_2 j \right] \omega \\
&- j \cdot \frac{\rho a}{A_i} \tan\left(\omega \frac{L_i}{a}\right) + \left[-\frac{\rho(\zeta_2 - D)}{A_e^2} \bar{Q}_2 - \frac{\rho \zeta_T}{A_i^2} \bar{Q}_1 \right] = 0 \quad (22)
\end{aligned}$$

Eq. (22) is a transcendential equation in terms of ω. From the characteristic equation (22), we can determine the complex frequency $\omega = \omega_R + j\omega_I$. The expression $e^{j\omega t} = e^{j\omega_R t} \cdot e^{-\omega_I t}$ shows that the real part ω_R gives the frequency and the imaginary part ω_I the damping rate.

When $\left| \omega \frac{L_i}{a} \right| \ll 1$, $\tan\left(\omega \frac{L_i}{a}\right) \approx \omega \frac{L_i}{a}$ and $j \cdot \frac{\rho a}{A_i} \tan\left(\omega \frac{L_i}{a}\right) \approx \frac{\rho L_i}{A_i} j\omega$. For this case, the characteristic equation is reduced to a third order equation, which has been obtained for incompressible flow in the penstock [1].

Equation (21) can be written as

$$\rho C \frac{L_e}{A_e} \frac{d^2 \tilde{Q}_2}{dt^2} + \rho C \frac{\zeta_2 - D}{A_e^2} \bar{Q} \frac{d\tilde{Q}_2}{dt} + \tilde{Q}_2 = \tilde{Q}_1 + 2\rho C \alpha \frac{\cot \beta_2}{S} \left(\frac{\cot \beta_2}{S} \bar{Q} - U_2 \right) \frac{d\tilde{Q}_1}{dt} \quad (23)$$

If we consider the case of $\tilde{Q}_1 = 0$, negative damping occurs when $D > \zeta_2$. This is caused by the diffuser effect of the draft tube. The draft tube resonance frequency is given by

$$\omega_e = \sqrt{\frac{A_e}{\rho L_e C}} \quad (24)$$

RESULTS AND DISCUSSION

Due to the term of $j \cdot \frac{\rho a}{A_i} \tan\left(\omega \frac{L_i}{a}\right)$, the characteristic equation (22) is a transcendental equation, having higher order solutions. An iterative method is used to solve Eq. (22). The values of the parameters used for sample calculations are given in the nomenclature. These values are determined by considering a test facility at EPFL and used for sample calculation as standard values except for the parameters specified for each case. The value of the loss coefficient ζ_T representing the effect of the runner was determined by assuming that the applied head H equals to $(\zeta_T / 2g)(\overline{Q} / A_i)^2$. The value of the cavitation compliance C was determined so that the frequency given by Eq.(24) becomes 0.16 times the rotational speed of the runner $f_n = 12.5Hz$. The swirl free flow rate Q_{sf} which gives no swirl at the runner exit is calculated to be $Q_{sf} = S \cdot U_2 \tan \beta_2 = 0.618 m^3 / s$.

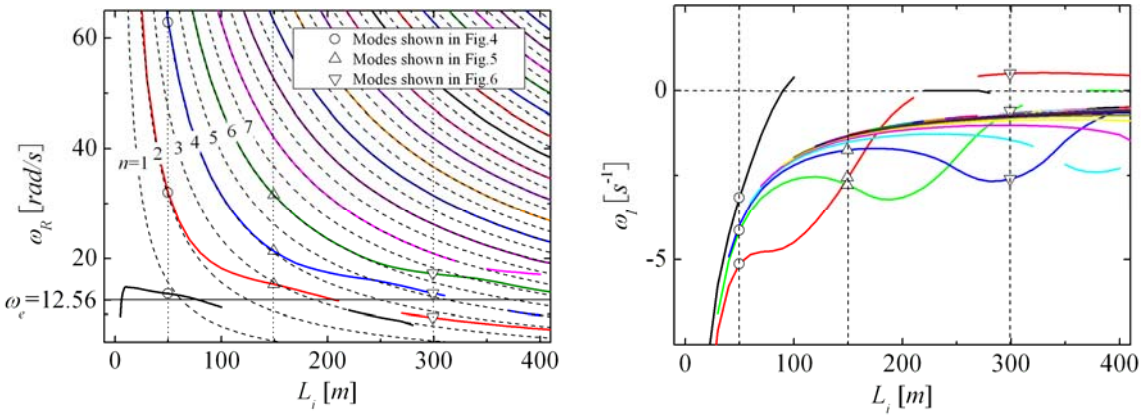

Fig. 3 Higher order frequencies under *a* = 500 m/s

Effect of inlet pipe length L_i. Fig. 3 shows the solutions when the wave speed is a = 500 m/s for the standard condition shown in the nomenclature. The mean flow rate $\overline{Q}$=0.51 m^3/s is smaller than the swirl free flow rate Q_{sf}=0.618 m^3/s. The full line curves represent different order modes. The draft tube resonant frequency $\omega_e = \sqrt{A_e/(\rho L_e C)} = 12.56\ rad/s$ is also shown in Fig.3. The multiple quarter wavelength resonance frequencies $\omega_n = 2\pi na/4L_i$ of the penstock are also plotted as dashed lines. We observe the followings in the figure:

1) At frequencies higher than about twice the draft tube frequency $2\omega_e$, the frequency obtained agrees with ω_n with even number of n. It will be shown later that these correspond to open to open resonant frequencies of the penstock.

2) As the frequencies approach the draft tube resonant frequency ω_e, the obtained frequencies deviates from ω_n in the direction away from ω_n. This is opposite to the "lock in" phenomena observed for Karman vortex from flexibly supported cylinders.

3) When $\overline{Q} < Q_{sf}$, most of the modes have negative damping (ω_I <0).

At L_i = 50m, 150m and 300m the lowest 3 mode frequencies are listed in Table 1 and the velocity and pressure fluctuation modes in Fig.4 to 6. The corresponding frequencies are shown in Fig. 3. At L_i = 50m, the fluctuations of 1st mode has about 1/4 wavelength, and 2nd and 3rd order are about 1/2 and 1 wavelength respectively, as expected from the comparison with the multiple quarter wavelength frequencies shown in Fig.3. At L_i = 50m and 150m, for the 1st order mode with the frequency closer to ω_e, the runner inlet is a node of velocity fluctuation. However, the runner inlet is a loop for higher order modes. At L_i = 300 m, the runner inlet is a node of velocity fluctuation for the 2nd order mode, whose frequency is closer to ω_e than other order frequencies. The 1st order mode with the frequency less than ω_e is a damping mode as shown in Fig.3 and Table 1.

Table 1 First 3 order frequencies at L_i =50 m, 150 m and 300 m

order	Frequency ω		
	L_i =50 m	L_i =150 m	L_i =300 m
1	13.683 - 3.158 j	15.335 - 2.561 j	9.381 + 0.504 j
2	31.909 - 5.126 j	21.256 - 2.787 j	13.763 - 0.597 j
3	62.937 - 4.140 j	31.465 - 1.753 j	17.274 - 2.606 j

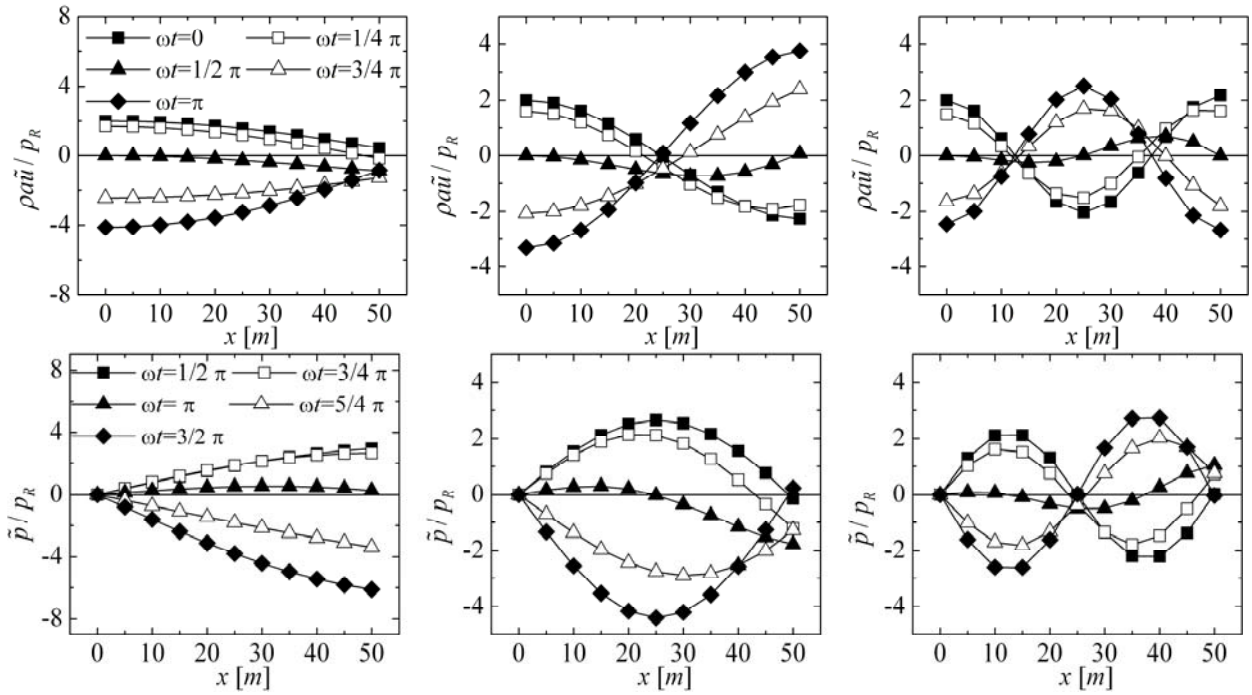

ω_1 =13.683 - 3.158 j ω_2 =31.909 - 5.126 j ω_3 =62.937 - 4.140 j

Fig. 4 Velocity and pressure fluctuations along the inlet pipe at L_i = 50 m

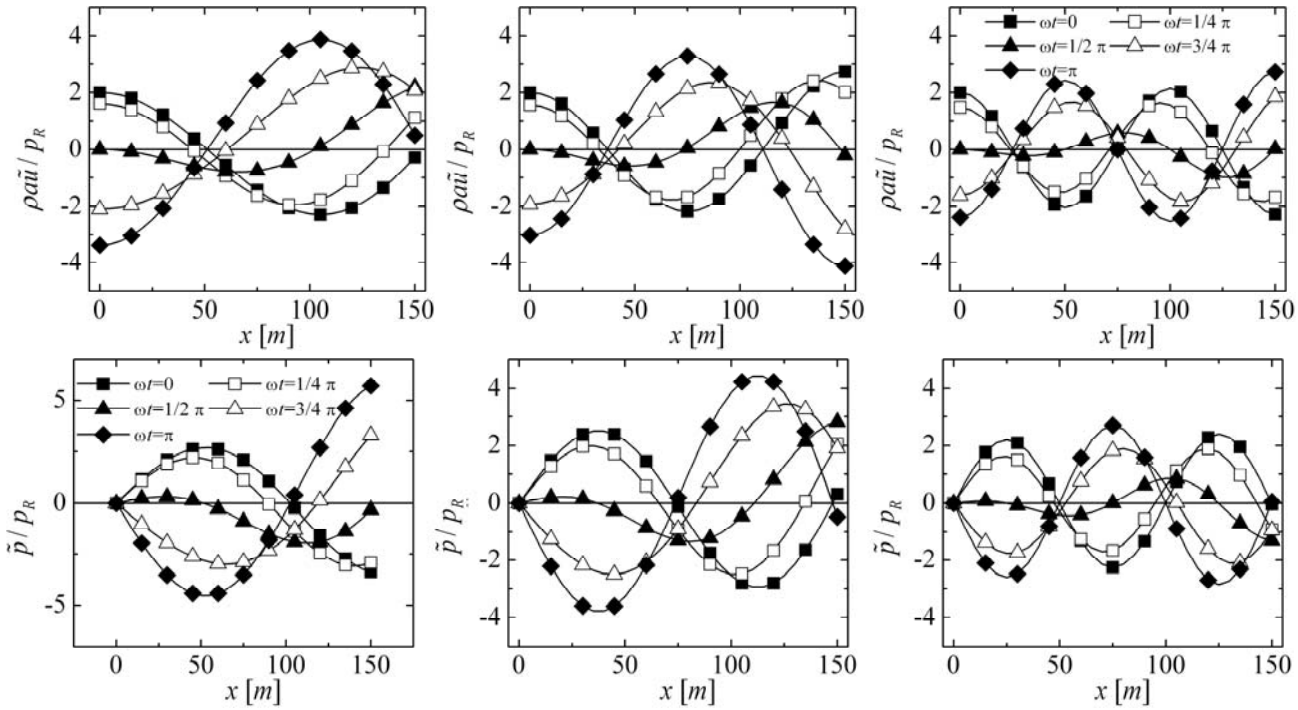

ω_1 =15.335 - 2.561 j ω_2 =21.256 - 2.787 j ω_3 =31.465 - 1.753 j

Fig. 5 Velocity and pressure fluctuations along the inlet pipe at L_i = 150 m

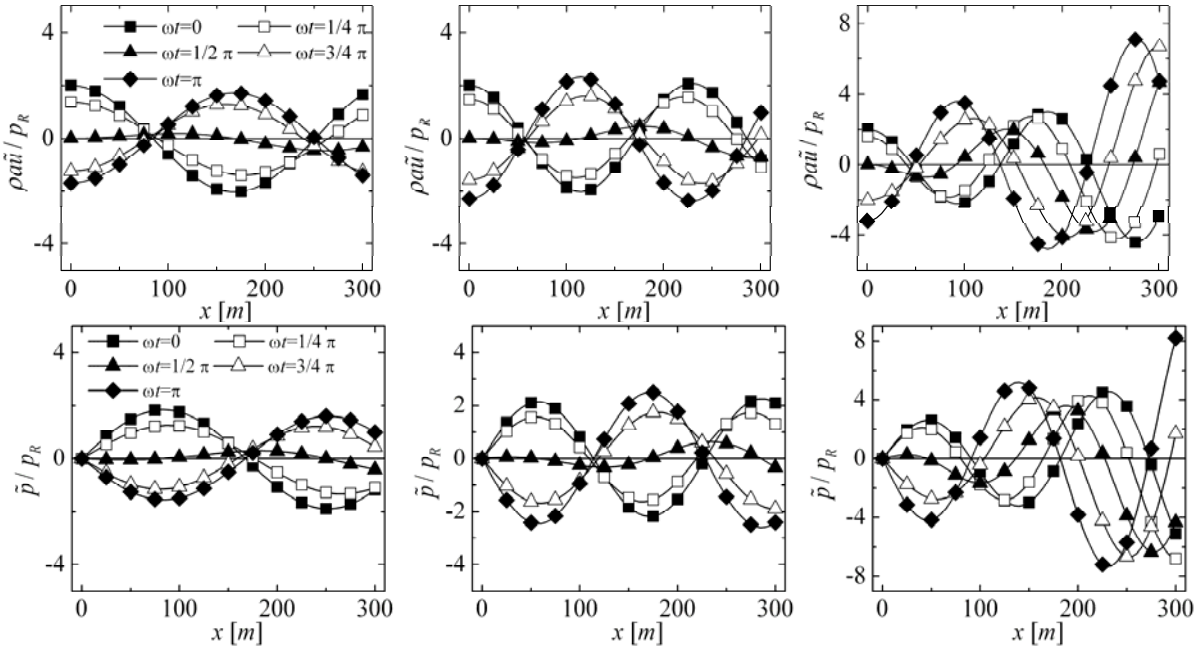

ω_1 =9.381 + 0.504 j ω_2 =13.763 - 0.597 j ω_3 =17.274 - 2.606 j

Fig. 6 Velocity and pressure fluctuations along the inlet pipe at L_i = 300 m

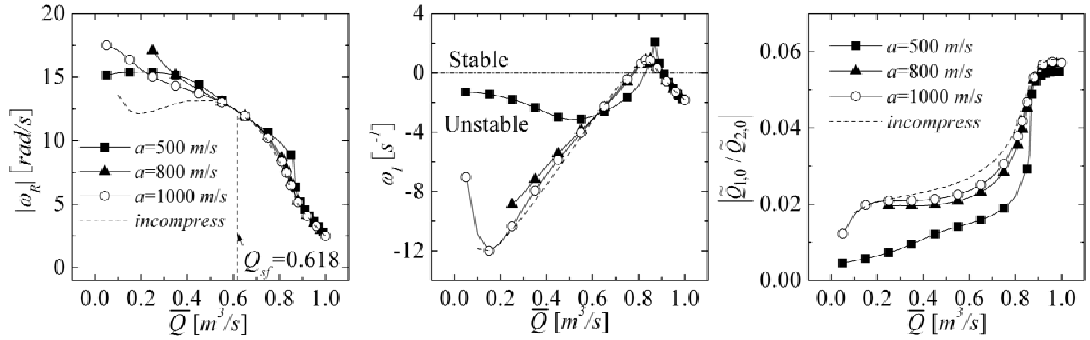

Fig. 7 Effect of mean flow rate $\bar{Q}$ under standard condition (L_i =50 m)

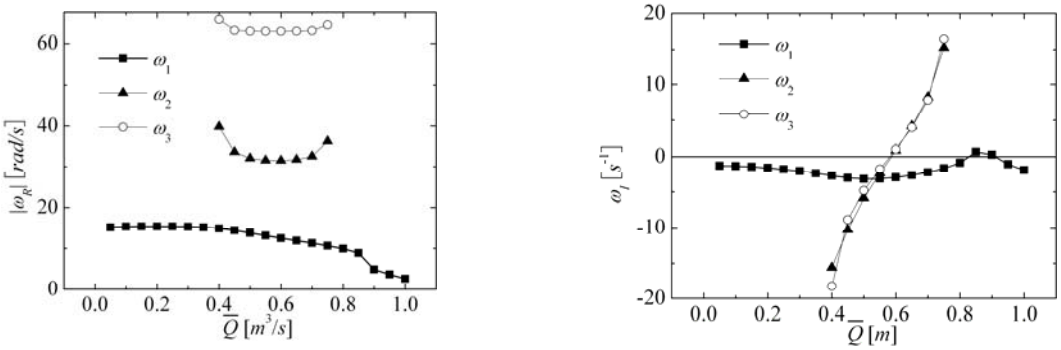

Fig. 8 Effect of $\bar{Q}$ to first 3 order frequencies at *Li* = 50 m, under *a* = 500 *m/s*

Effects of mean flow rate and contributions of diffuser and swirl effects. We consider the lowest order mode with the frequency close to ω_e for L_i =50m firstly. Fig. 7 shows the results under standard condition with three different values of wave speed *a*. Although we observe some effects of the wave speed, general characteristics are not affected by the wave speed.

Fig. 8 shows the effects of mean flow rate on the lowest 3 frequencies under a = 500 m/s. The real parts of 2nd order frequency ω_2 and 3rd order frequency ω_3 increase as the flow rate departs from the swirl free flow rate Q_{sf}. While ω_1 shows negative damping in a wider region of mean flow rate, ω_2 and ω_3 have negative damping in the region of $\bar{Q} < Q_{sf}$.

We examine the diffuser and swirl effects separately by putting $\alpha = 0$ or D-ζ_2 =0. Fig. 9 shows the results for Li = 50 m and a = 500 m/s. With $\alpha = 0$, ω_2 and ω_3 are always damping without the effect of value of D. This shows that the diffuser effect does not cause higher order modes in the penstock. With D-ζ_2 =0 and larger values of α, all modes have negative / positive damping for $\bar{Q}$ </> Q_{sf}. This shows that the swirl effect affects all modes and causes instabilities when $\bar{Q} < Q_{sf}$.

The effects of swirl and diffusion at Li =150 m are shown in Fig.10. Fig.3 shows that the lowest order frequency ω_1 at Li =150 m corresponds to the second order frequency ω_2 at Li =50m. This is also shown in Figs.4 and 5 for the 1st order mode. However, comparing Figs.9 and 10, the results of Li=150m for ω_1 are similar to the results for ω_1 of Li =50m, with the values of ω_1 close to ω_e for both cases. The diffuser still has a significant effect on ω_1 but little on ω_2 and ω_3. This shows that the diffuser effect affects the modes with the resonant frequency close to ω_e, independently on the mode shape in the penstock. On the other hand, swirl has larger effect on all of the lowest 3 frequency modes.

Table 2 First 3 order frequencies and mode under α = 0, D = 0.5D_{stand},

order	L_i =50 m		L_i =150 m		L_i =300 m	
	ω	$\tilde{Q}_{1,0} / \tilde{Q}_{2,0}$	ω	$\tilde{Q}_{1,0} / \tilde{Q}_{2,0}$	ω	$\tilde{Q}_{1,0} / \tilde{Q}_{2,0}$
1	12.574 -1.151j	-0.010 -0.006j	12.657 -1.004j	-0.0232-0.0299j	10.375+0.324j	0.3239-0.1991j
2	31.594+2.544j	-5.242 -1.495j	21.059+0.838j	-1.7912-0.5412j	12.536 -1.065j	-0.0041-0.0199j
3	62.912+2.563j	-23.983 -2.991j	31.476+0.852j	-5.2567-0.8144j	15.824+0.386j	-0.5789-0.3161j

The smaller diffuser effect on higher order frequencies may be explained by the draft tube resonance frequency ω_e =12.56 Hz. Table 2 shows $\tilde{Q}_{1,0} / \tilde{Q}_{2,0}$ for each case with the values of ω. $\tilde{Q}_{1,0}$ and $\tilde{Q}_{2,0}$ are flow rate fluctuations at the runner inlet and outlet. For the cases with ω_1 for L_i =50m and 150m and ω_2 for L_i =300m, the frequencies are closer to ω_e. For these cases $\left|\tilde{Q}_{1,0} / \tilde{Q}_{2,0}\right|$ has smaller values suggesting that oscillations in the draft tube is much larger. For these cases the effects of D is significant. For other cases, $\tilde{Q}_{1,0} / \tilde{Q}_{2,0}$ has larger values suggesting larger amplitude of oscillations in the penstock.

We also check the diffuser and swirl effect at L_i = 300 m in Fig.11. The diffuser has larger effect on ω_2 but little on ω_1 and ω_3. This is because ω_2 is the nearest value to the draft tube resonance frequency ω_e at L_i = 300 m, as listed in Table 1. The swirl effect on the 1st order mode with the frequency less than ω_e is totally different from other cases. This will be discussed later.

Comparing Figs.9 to 11, for the diffuser effects (α=0), only the modes with the frequency closest to the draft tube resonant frequency ω_e are affected and the instability is caused. Other modes with the frequencies far from ω_e are not affected nor destabilized by the diffuser effect.

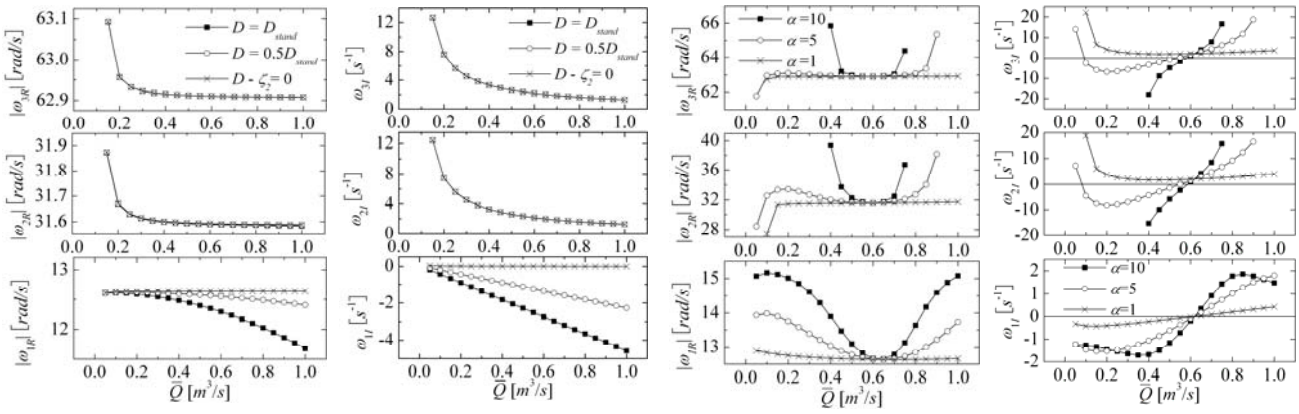

a) α=0 b) $D - \zeta_2 = 0$

Fig. 9 Diffuser and swirl effects to lowest 3 frequencies at *Li* = 50 m, *a* = 500 *m/s*

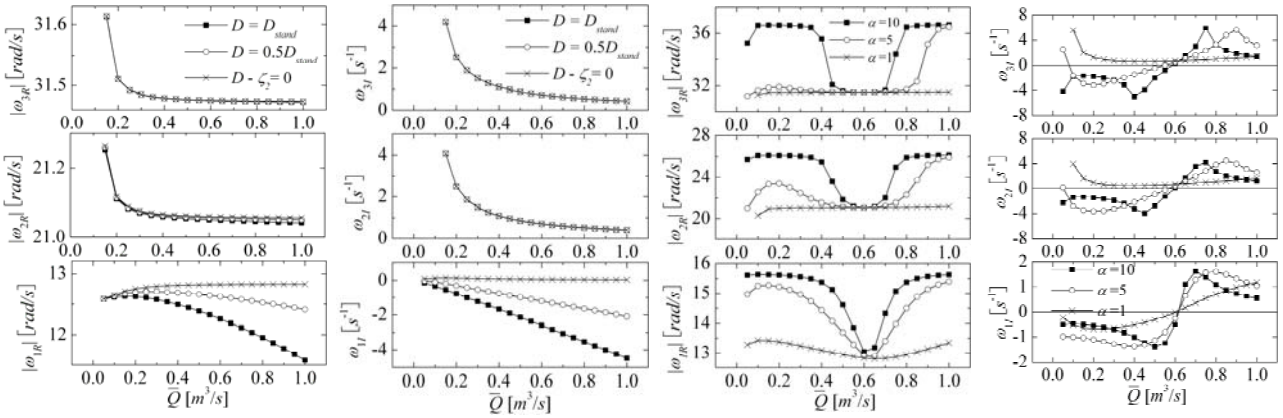

a) α=0 b) $D - \zeta_2 = 0$

Fig. 10 Diffuser and swirl effects to lowest 3 order frequencies at *Li* = 150 m, *a* =500 *m/s*

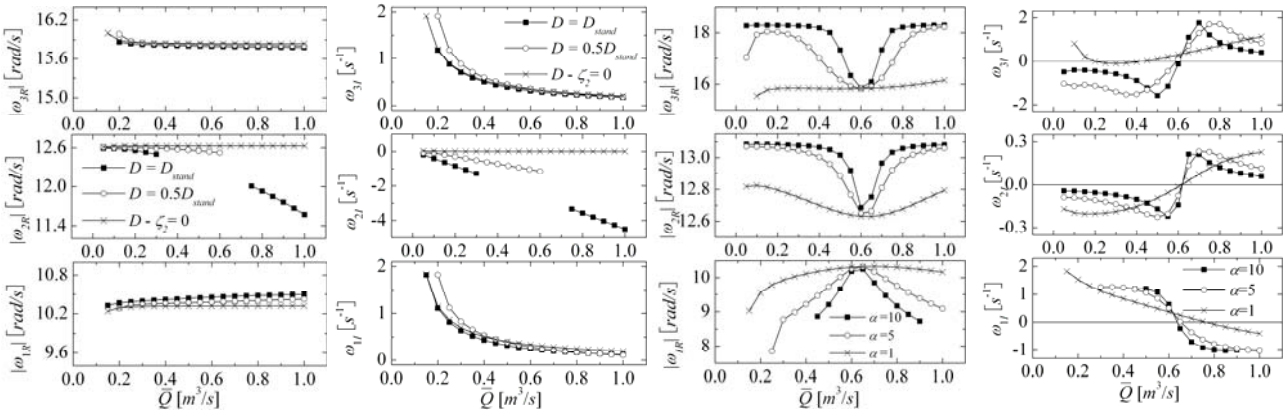

a) α=0 b) $D - \zeta_2 = 0$

Fig. 11 Diffuser and swirl effects to lowest 3 order frequencies at *Li* = 300 m, *a* = 500 *m/s*

On the other hand, the swirl effects (D-$\zeta_2 = 0$) affects all modes except for the first order mode of L_i = 300m, which has a resonant frequency lower than ω_e, and destabilizes them at $\bar{Q} < Q_{sf}$. The destabilizing swirl effect for the general case is explained as follows. Consider the case when the upstream flow rate Q_1 increases under the mean flow rate $\bar{Q} </> Q_{sf}$. Then the swirl velocity decreases / increases and the pressure in the vortex core is increased / decreased. This results in decreased / increased cavity volume V_C. From the continuity equation $dV_C/dt = Q_2 - Q_1$, Q_2 will be decreased / increased and Q_1 will be increased / decreased for the general cases. This means that the cavity volume fluctuation provides positive / negative feed back at the mean flow rate $\bar{Q}$ smaller / larger than the swirl free flow rate Q_{sf}.

Fig.12 shows the plot of $\tilde{Q}_{1,0}/\tilde{Q}_{2,0}$ for the cases of D-ζ_2=0, α=5, L_i =150m and 300m. Almost for all cases, $\left|\tilde{Q}_{1,0}/\tilde{Q}_{2,0}\right| \ll 1$. For these cases, the cavity volume fluctuation is delayed behind the $\tilde{Q}_2$ fluctuation by about 90°, from the continuity relation $\tilde{Q}_2 = dV_c / dt$. Except for the case of $\omega_1 < \omega_e$ with L_i = 300m, $\mathrm{Real}\left(\tilde{Q}_{1,0}/\tilde{Q}_{2,0}\right) < 0$ and the phase difference between $\tilde{Q}_{1,0}$ and $\tilde{Q}_{2,0}$ is larger than ±90°. For this case upstream flow rate is decreased ($\tilde{Q}_{1,0}$ <0) when the cavity volume is increasing (dV_c / dt>0), as assumed in the discussion above. For the case of $\omega_1 < \omega_e$ with L_i =300m, $\mathrm{Real}\left(\tilde{Q}_{1,0}/\tilde{Q}_{2,0}\right) > 0$ and the phase difference between $\tilde{Q}_{1,0}$ and $\tilde{Q}_{2,0}$ is smaller than ±90°. In this case, both upstream and downstream flow rates becomes positive when dV_c / dt >0. This is opposite to the assumption in the above discussion. The positive feedback and the instability occur for the flow rates larger than the swirl free flow rate. The relationship between the cavity volume and flow rate fluctuation is shown in Fig.13 for the typical cases with phase difference equals to 180° (general cases) or 0° (for ω_1 with L_i =300m).

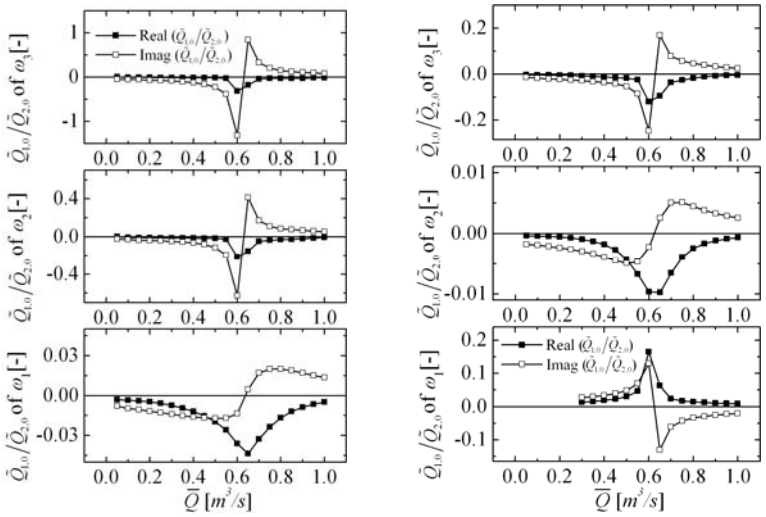

L_i =150 m L_i =300 m

Fig. 12 Modes of first 3 order frequencies at D -ζ_2 = 0 and α=5

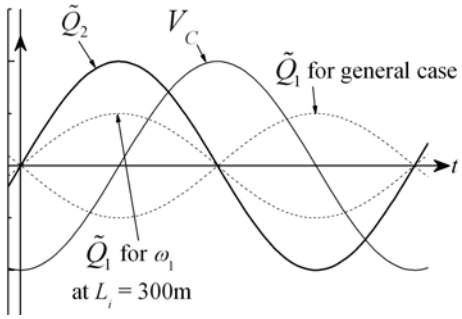

Fig. 13 Relationship among flow rate fluctuations and cavity volume

CONCLUSION

It was shown that various acoustic modes in the penstock can be destabilized by diffuser and swirl effects. At higher frequency than the draft tube resonant frequency ω_e, open-to-open acoustic modes occur in the penstock, when the flow rate is smaller than swirl free flow rate Q_{sf}. When the frequency of acoustic modes gets closer to ω_e, the oscillation frequency has a tendency to depart from ω_e. The diffuser effect of draft tube affects only the modes with the frequency closest to ω_e and causes the instability at all flow rates. For these modes, the flow rate fluctuation in the upstream of the runner is much smaller than the downstream and the velocity node occurs at the runner inlet. The swirl effect affects all modes and cause instability at smaller flow rates than Q_{sf}, except for the mode with the frequency less than ω_e. Thus, the higher order modes are caused by swirl effect. For the modes with the frequency less than ω_e, the phase difference between upstream and downstream flow rate fluctuation becomes less than 90° and the instability occurs at higher flow rate than Q_{sf}.

BIBLIOGRAPHICAL REFERENCES

[1] Chen, C., Nicolet, C., Yonezawa, K., Farhat, M., Avellan, F., Tsujimoto, Y., 2008,

One-Dimensional Analysis of Full Load Draft Tube Surge, ASME Trans. J. Fluids Eng., 130, 041106(2008).
[2] Jacob, T., Prenat, J-E., 1996, *Francis Turbine Surge: Discussion and Data Base*, Proc. 18th IAHR Symposium, Valencia, Spain.
[3] Nishi, M., 1984, *Surging Characteristics of Conical and Elbow Type Draft Tubes*, Pro. 12th IAHR Symposium on Hydraulic Machinery and System, Stirling, pp. 272-283.
[4] Nishi, M., Matsunaga, S., Kubota, T., Senoo, Y., 1982, *Flow Regimes in an Elbow-Type Draft Tube*, Proc. 11th IAHR Symposium on Hydraulic Machinery and System, Amsterdam, pp. 1-13, paper 38.
[5] Nishi, M., Wang, X., Okamoto, M., Matsunaga, S., 1994, *Further Investigation on the Pressure Fluctuations Caused by Cavitated Vortex Rope in an Elbow Draft Tube*, Cavitation and Gas Fluid Flow Machinery and Devices, ASME, pp. 63-70.
[6] Koutnik, J., Pulpitel, L., *Modeling of the Francis Turbine Full-Load Surge*, Modeling, Testing and Monitoring for Hydro Power Plants, Lausanne, 1996.
[7] Koutnik, J., Nicolet, C., A.Schoul, G., Avellen, F., *Overload Surge Event in a Pumped- Storage Power Plant*. In Proceeding of the 23rd IAHR Symposium, Yokohama, 2006, paper 135.
[8] Susan-Resiga, R., Ciocan, G.D., Anton, I., Avellan, F., 2006, *Analysis of the Swirling Flow Downstream a Francis Turbine Runner*, J. Fluid Eng., 128, pp. 177-189.